J. Fluid Mech. (1990), *vol.* 214, *pp.* 211–228
Printed in Great Britain

Two-dimensional shear dispersion for skewed flows in narrow gaps between moving surfaces

By RONALD SMITH

Department of Mathematical Sciences, University of Technology, Loughborough LE11 3TU, UK

(Received 24 April 1989 and in revised form 24 October 1989)

Flows transporting material between nearby moving surfaces are ubiquitous in machinery of all scales and with a variety of geometries. Here a general derivation is given of the effective two-dimensional mixing process in a narrow gap for a solute or miscible fluids. Explicit formulae are given for the shear dispersion tensor in laminar and turbulent (logarithmic velocity profile) flows. It is shown that if improved mixing is required, then the optimum direction for additional boundary motion or stress is at right angles to the primary flow direction.

1. Introduction

In the atmosphere the wind direction varies with height above the ground. This profoundly affects the travel path and rate of spread of pollution in the atmosphere, particularly for ground-level releases. It is often appropriate to regard the flow as being horizontally uniform. The method of moments (Aris 1956) can then be used to calculate the concentration distribution (Saffman 1962; Smith 1965; Csanady 1969; Taylor 1982). At large distances downstream (of order 100 km), when the pollution has become uniform across the well-mixed layer (typical depth 1 km), the dispersion process becomes two-dimensional.

In the oceans the velocity direction can likewise vary with depth, either because of the Earth's rotation (the Ekman spiral) or because of non-alignment between wind and tidal forcing. For coastal waters, vertical mixing takes place over comparatively short distances (of order 1 km). Fischer (1978) gives a direct derivation of the two-dimensional dispersion process for a skewed shear flow. He showed that there is a tensor shear dispersion coefficient involving the two horizontal velocity components. The particular problem of concern to Fischer (1978) was pollution transport and dilution in waters over a flat part of the Atlantic continent shelf of the United States. This led him to restrict his attention to uniform Cartesian geometry and to use a site-specific empirical velocity profile. Smith (1979) evaluated the shear dispersion tensor for buoyant contaminants, while Hamrick (1986) evaluated the tidally averaged shear dispersion tensor.

Narrow-gap skewed shear flows carrying material can also occur in machinery of all sizes, from oil lubricating bearings as small as 1 mm, to water slurries at the face and around the circumference of tunnel boring machines of 10 m diameter. Unlike the geophysical applications, the gap widths vary markedly, and the geometries are rarely Cartesian. The first objective of the present paper is to give a derivation of the two-dimensional shear dispersion equation that is free from geometrical restrictions. The second objective is to evaluate the shear dispersion tensor for laminar and for

turbulent (logarithmic velocity profile) flows, i.e. tensor counterparts to the scalar shear dispersion coefficients derived by Taylor (1953) and by Elder (1959).

A useful general principle revealed by the analysis is that to encourage good mixing there should be motion perpendicular to the main flow direction. For example, it is indeed appropriate that the axial transport of slurry back along the circumference of a tunnel boring machine should be accompanied by rotation of the outer surface.

2. Narrow-gap equations for density and concentration

As sketched in figure 1, the normal distance from a reference surface S (e.g. a cylinder of radius a) is written n. The three-dimensional gradient operator is approximated

$$(\boldsymbol{\nabla}_S, \partial_n) \tag{2.1}$$

where $\boldsymbol{\nabla}_S$ is the two-dimensional operator on the reference surface. It is by suppressing the n-dependence of $\boldsymbol{\nabla}_S$ that the following equations are approximate not exact. For example, in cylindrical polar coordinates we approximate

$$\frac{1}{a+n}\frac{\partial}{\partial\theta} \quad \text{by} \quad \frac{1}{a}\frac{\partial}{\partial\theta}. \tag{2.2}$$

The three-dimensional velocity field is decomposed:

$$(\boldsymbol{u}_S, w), \tag{2.3}$$

where $\boldsymbol{u}_S$ is a vector in the reference surface, and w is the much smaller velocity across the narrow gap.

The miscible fluids involved in shear-augmented mixing need not have the same density, So, we shall allow the density ρ to vary. The mass conservation equation is

$$\partial_t \rho + \boldsymbol{\nabla}_S \cdot (\rho \boldsymbol{u}_S) + \partial_n(\rho w) = 0. \tag{2.4}$$

We characterize the mixing process in terms of the mass fraction c of the solute or the intruding fluid. The density, diffusivity and viscosity would typically be functions of c. The advection–diffusion equation for c takes the form

$$\rho\,\partial_t c + \rho \boldsymbol{u}_S \cdot \boldsymbol{\nabla}_S c + \rho w\,\partial_n c = \boldsymbol{\nabla}_S \cdot (\rho \boldsymbol{\kappa}_S \cdot \boldsymbol{\nabla}_S c) + \partial_n(\rho\kappa\,\partial_n c). \tag{2.5}$$

For simplicity it has been assumed that the outwards normal is one of the principal directions of the diffusivity tensor. The magnitude of this normal diffusivity is denoted by the scalar κ. The other tensor components within the surface are denoted $\boldsymbol{\kappa}_S$. In a laminar flow of a Newtonian fluid $\boldsymbol{\kappa}_S$ would be isotropic with scalar diffusivity κ. For a turbulent flow equation (2.5) is merely an empirical model, with the advantage of established parameterizations for the eddy diffusivities, $\kappa, \boldsymbol{\kappa}_S$. The narrowness of the gap means that the right-hand side of (2.5) is dominated by the n-derivatives.

We denote the outer interface by

$$n = N^{(+)}(\boldsymbol{x}, t), \tag{2.6}$$

where $\boldsymbol{x}$ denotes the two-dimensional position on the reference surface S. The condition for zero mass flux across the boundary is

$$w = \partial_t N^{(+)} + \boldsymbol{u}_S \cdot \boldsymbol{\nabla}_S N^{(+)} \quad \text{on} \quad n = N^{(+)}. \tag{2.7}$$

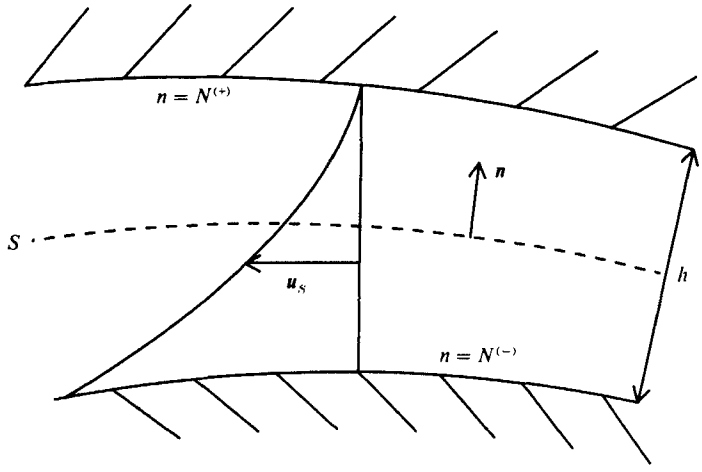

FIGURE 1. Definition sketch showing the reference surface S, the normal distance n, and the boundaries $n = N^{(-)}, n = N^{(+)}$ separated by the narrow-gap width h.

For the concentration we need to allow for the diffusive flux:

$$wc - \kappa \partial_n c = c\,\partial_t N^{(+)} + (\boldsymbol{u}_S c - \boldsymbol{\kappa}_S \cdot \boldsymbol{\nabla}_S c)\cdot \boldsymbol{\nabla}_S N^{(+)} \quad \text{on} \quad N = N^{(+)}. \tag{2.8}$$

These equations can be derived from the mass or species budget in a coin-shaped control volume with the upper surface moving with the impermeable interface $N^{(+)}$. The narrowness of the gap and the smallness of w means that the n-derivative is very much the dominant term in (2.8). On the inner boundary $n = N^{(-)}$ it suffices that we replace the $^{(+)}$ superscripts by $^{(-)}$.

3. Averaging across the gap

Since the gap is narrow, the concentration will rapidly become nearly uniform across the gap. The subsequent mixing process will be two-dimensional. Following Fischer (1978, equation 3) we use averaging across the gap to derive two-dimensional counterparts to (2.3), (2.4).

We denote the gap width by

$$h = N^{(+)} - N^{(-)}. \tag{3.1}$$

Average values across the gap are denoted $\|\ldots\|$:

$$\|f\| = \frac{1}{h}\int_{N^{(-)}}^{N^{(+)}} f \,\mathrm{d}n. \tag{3.2}$$

The natural two-dimensional flow properties involve a mass-weighting:

$$\boldsymbol{U}_S = \frac{1}{\|\rho\|}\|\rho \boldsymbol{u}_S\|, \quad C = \frac{1}{\|\rho\|}\|\rho c\|, \quad \boldsymbol{K}_S = \frac{1}{\|\rho\|}\|\rho \boldsymbol{\kappa}_S\|. \tag{3.3a, b, c}$$

With these definitions there are striking similarities between (2.4), (2.5) and their integrated counterparts:

$$\partial_t(h\|\rho\|) + \boldsymbol{\nabla}_S \cdot (h\|\rho\|\,\boldsymbol{U}_S) = 0, \tag{3.4}$$

$$h\|\rho\|\,\partial_t C + h\|\rho\|\,\boldsymbol{U}_S \cdot \boldsymbol{\nabla}_S C = \boldsymbol{\nabla}_S \cdot (h\|\rho\|\boldsymbol{K}_S \cdot \boldsymbol{\nabla}_S C) + \boldsymbol{\nabla}_S \cdot (h\|\rho(\boldsymbol{U}_S - \boldsymbol{u}_S)(c - C)\|) + \boldsymbol{\nabla}_S \cdot (h\|\rho(\boldsymbol{\kappa}_S - \boldsymbol{K}_S)\cdot \boldsymbol{\nabla}_S (c - C)\|). \tag{3.5}$$

In effect, the integration across the gap and the use of the boundary conditions (2.7), (2.8) replaces the ∂_n terms in (2.4), (2.5) by ∇_S terms. It is only in the final two terms in (3.5) that there is any dependence upon the concentration profile across the gap.

These same equations (3.4), (3.5) can be derived even if the gap is wide. However, depending upon the geometry of the reference surface, S, interpretation of h, $\|...\|$ and ∇_S would have to be modified to accommodate the n-dependence. For example, if S is a cylinder of radius a, then we would replace the notation (3.1), (3.2) by

$$h = \frac{1}{a}\int_{a+N^{(-)}}^{a+N^{(+)}} r\,\mathrm{d}r = (N^{(+)}-N^{(-)})\left[1+\frac{(N^{(+)}+N^{(-)})}{2a}\right], \tag{3.6a}$$

$$h\|f\| = \frac{1}{a}\int_{a+N^{(-)}}^{a+N^{(+)}} fr\,\mathrm{d}r = \int_{N^{(-)}}^{N^{(+)}}\left(1+\frac{n}{a}\right)f\,\mathrm{d}n. \tag{3.6b}$$

So, for (3.4), (3.5) the narrow-gap approximation can be regarded as simplifying the evaluation of h and $\|...\|$.

For later use we note that, in the narrow-gap limit, an integration by parts with respect to n yields the identity

$$\|\rho(\boldsymbol{U}_S-\boldsymbol{u}_S)(c-C)\| = -\left\|\partial_n c\int_{N^{(-)}}^{n}\rho(\boldsymbol{U}_S-\boldsymbol{u}_S)\,\mathrm{d}n'\right\|. \tag{3.7}$$

4. Concentration profile across the narrow gap

The profound contribution of G. I. Taylor (1953) in his analysis of unidirectional flows, was to recognize the importance of the $\rho(\boldsymbol{U}_S-\boldsymbol{u}_S)(C-c)$ term in (3.5). Although it is small relative to the left-hand-side advection term, the physical character is diffusive not advective. So, if the diffusion is weak (Péclet numbers in excess of unity based upon the gap width), the shear contribution can be large relative to $\boldsymbol{K}_S$. Hence, it is necessary to seek a higher approximation to the concentration profile across the flow:

$$c = C+c' \quad \text{with} \quad c' \ll C \quad \text{and} \quad \|\rho c'\| = 0. \tag{4.1}$$

By contrast, when c' is small it is justifiable to neglect the $\rho(\boldsymbol{\kappa}_S-\boldsymbol{K}_S)\nabla_S(C-c)$ term in (3.5), because it does not account for any physical effects not already represented by larger terms.

If we use (3.5) to eliminate $\partial_t C$, then the exact equation for c' can be written

$$\begin{aligned}&\rho\,\partial_t c'+\rho\boldsymbol{u}_S\cdot\nabla_S c'+\rho w\,\partial_n c'-\nabla_S(\rho\boldsymbol{\kappa}_S\cdot\nabla_S c')-\partial_n(\rho\kappa\,\partial_n c')\\&\quad+\frac{\rho}{h\|\rho\|}\{\nabla_S\cdot(h\|\rho(\boldsymbol{U}_S-\boldsymbol{u}_S)c'\|)+\nabla_S\cdot(h\|\rho(\boldsymbol{\kappa}_S-\boldsymbol{K}_S)\cdot\nabla_S c'\|)\}\\&=\rho(\boldsymbol{U}_S-\boldsymbol{u}_S)\cdot\nabla_S C+\nabla_S\cdot(\rho\boldsymbol{\kappa}_S\cdot\nabla_S C)-\frac{\rho}{\|\rho\|}\nabla_S\cdot(\|\rho\|\boldsymbol{K}_S\cdot\nabla_S C).\end{aligned} \tag{4.2}$$

The density and diffusivities would be functions of the local concentration $C+c'$.

Following Taylor (1953) we make drastic simplifications to both sides of this equation. On the left-hand side of (4.2) the first three terms comprise the advective rate of change, which we shall assume is small compared with the timescale for mixing across the narrow gap. The next term involves gradients ∇_S along and around the gap, which are small relative to gradients ∂_n across the gap. Similarly, the

$(\boldsymbol{U}_S - \boldsymbol{u}_S)c'$ and $\boldsymbol{\kappa}_S - \boldsymbol{K}_S$ terms are small by virtue of the $\boldsymbol{\nabla}_S$ gradients. On the right-hand side we ignore the $\boldsymbol{\kappa}_S$ and $\boldsymbol{K}_S$ terms on the basis that longitudinal advection dominates longitudinal diffusion (i.e. it is when diffusion is weak that the shear effect needs to be calculated). The much simplified equation for c' is

$$-\partial_n(\rho\kappa\,\partial_n c') = \rho(\boldsymbol{U}_S - \boldsymbol{u}_S)\cdot\boldsymbol{\nabla}_S C. \tag{4.3}$$

A formal mathematical derivation in axes moving with the two-dimensional flow $\boldsymbol{u}_S$ (Smith 1979; Hamrick 1986) would require that the diffusivities κ, $\boldsymbol{\kappa}_S$, $\boldsymbol{K}_S$ are smaller than $|\boldsymbol{U}_S|a$ but larger than $|\boldsymbol{U}_S|h^2/a$, (i.e. small diffusion but not so small that there is not mixing across the narrow gap). The approximate boundary conditions are

$$\rho\kappa\,\partial_n c' = 0 \quad \text{on} \quad n = N^{(+)}, N^{(-)}. \tag{4.4}$$

A first integral is

$$-\rho\kappa\,\partial_n c' = \boldsymbol{\nabla}_S C \cdot \int_{N^{(-)}}^{n} \rho(\boldsymbol{U}_S - \boldsymbol{u}_S)\,\mathrm{d}n'. \tag{4.5}$$

5. Two-dimensional dispersion equation

In view of the identity (3.7), and the approximate solution (4.5) for $\partial_n c'$, we are now in a position to evaluate the shear terms in (3.5). The diffusive character is a consequence of the facts that the shear term is in divergence form and $\partial_n c'$ is proportional to $\boldsymbol{\nabla}_S C$. We define the tensor coefficients

$$\boldsymbol{D}_S = \frac{1}{\|\rho\|}\left\|\frac{1}{\rho\kappa}\boldsymbol{I}_S^{\mathrm{T}}\boldsymbol{I}_S\right\|, \tag{5.1a}$$

with

$$\boldsymbol{I}_S = \int_{N^{(-)}}^{n} \rho(\boldsymbol{U}_S - \boldsymbol{u}_S)\,\mathrm{d}n'. \tag{5.1b}$$

The T superscript indicates the transpose of a vector (from row to column form). These double integrals (5.1*a*) are a slight simplification upon the triple integrals derived by Fischer (1978, equation (8), and avoid the summation over eigenmodes used by Hamrick (1986, equation (63)).

With these definitions the shear-dispersion equation (3.5) for $C(\boldsymbol{x}, t)$, with the last term neglected, can be approximated:

$$h\|\rho\|\,\partial_t C + h\|\rho\|\,\boldsymbol{U}_S\cdot\boldsymbol{\nabla}_S C - \boldsymbol{\nabla}_S\cdot(h\|\rho\|[\boldsymbol{K}_S + \boldsymbol{D}_S]\cdot\boldsymbol{\nabla}_S C) = 0. \tag{5.2}$$

In the particular case of Cartesian geometry with uniformity with respect to both x and y, this agrees with the two-dimensional equation derived by Fischer (1978, equation (9)). The tensor variance grows at the rate $2(\boldsymbol{K}_S + \boldsymbol{D}_S)$, in agreement with the method of moments (Saffman 1962).

The importance of this Taylor (1953)-type of analysis, is that the shear dispersion coefficients $\boldsymbol{D}_S$ can be comparable with or even exceed the conventional diffusivities $\boldsymbol{K}_S$. Also, the values of the components of $\boldsymbol{D}_S$ can be evaluated via the explicit formulae (5.1*a*, *b*). Formally, $\boldsymbol{D}_S$ and $\boldsymbol{K}_S$ are of comparable magnitude if the diffusivities $\kappa, \boldsymbol{\kappa}_S$ are of order $|\boldsymbol{U}_S|h$, (i.e. Péclet numbers of order unity based upon the gap width).

6. Narrow-gap flow between moving boundaries

To evaluate the shear-dispersion tensor $\boldsymbol{D}_S$, we need to know the velocity profiles $\boldsymbol{u}_S(\boldsymbol{x}, n, t)$. Fischer (1978, figure 1) uses an empirical step profile for the transverse velocity and a linear profile for the longitudinal velocity while Hamrick (1986, equation (58)) solves for an eigenvector representation. Here we undertake the task of calculating the velocity profiles across the narrow gap between differentially moving boundaries.

We decompose the vertical gravitational acceleration vector (or other body force) into surface and normal components

$$(\boldsymbol{g}_S, g_n). \tag{6.1}$$

Since the gap is narrow, we shall neglect any n-dependence of these components. Across the gap, we assume that the pressure p is hydrostatic:

$$\partial_n p - \rho g_n = 0. \tag{6.2}$$

In particular, if the density is a function of the concentration c, then the approximation $c' \ll C$ permits us to regard ρ as being close to the average $\|\rho\|$. So, we approximate the pressure distribution:

$$p = \|p\| + \|\rho\| g_n (n - \|n\|). \tag{6.3}$$

Since the gap is narrow, the $\|p\|$-term dominates.

By analogy with the cross-stream diffusion equation (4.3), we approximate the momentum equations along and around the narrow gap:

$$\partial_n(\mu \partial_n \boldsymbol{u}_S) = \boldsymbol{\nabla}_S \|p\| - \|\rho\| \boldsymbol{g}_S, \tag{6.4}$$

where μ is the viscosity of the Newtonian fluid mixture. Thus, any departure from hydrostatic balance gives rise to flow, with effectively immediate adjustment of velocity profile across the narrow gap. The advective transport of momentum can be neglected provided that μ is larger than $\rho|\boldsymbol{U}_S|h^2/a$ (Reynolds' number based on the gap width of less than a/h). At the boundaries the tangential velocity matches to the motion of the solid boundaries:

$$\boldsymbol{u}_S = \boldsymbol{u}^{(+)} \quad \text{on} \quad n = N^{(+)}, \tag{6.5a}$$

$$\boldsymbol{u}_S = \boldsymbol{u}^{(-)} \quad \text{on} \quad n = N^{(-)}. \tag{6.5b}$$

In geophysical flows it would be necessary to include Coriolis terms in the momentum equation (6.4).

It is convenient to decompose the velocity field $\boldsymbol{u}_S$ into those contributions associated with the bulk flow $\boldsymbol{U}_S$ and with the boundary motions $\boldsymbol{u}^{(+)}, \boldsymbol{u}^{(-)}$:

$$\boldsymbol{u}_S = \boldsymbol{U}_S f^{(0)}(n) + \boldsymbol{u}^{(+)} f^{(+)}(n) + \boldsymbol{u}^{(-)} f^{(-)}(n). \tag{6.6}$$

In particular, for a laminar flow with constant μ, we have (see figure 2)

$$f^{(0)} = 6\xi(1-\xi), \quad f^{(+)} = -2\xi + 3\xi^2, \tag{6.7a, b}$$

$$f^{(-)} = 1 - 4\xi + 3\xi^2, \quad \text{with} \quad \xi = \frac{n - N^{(-)}}{h}. \tag{6.7c, d}$$

For turbulent flows the range of sizes of the eddies involved in the transport across the gap of momentum (or concentration) increases away from the boundaries. This

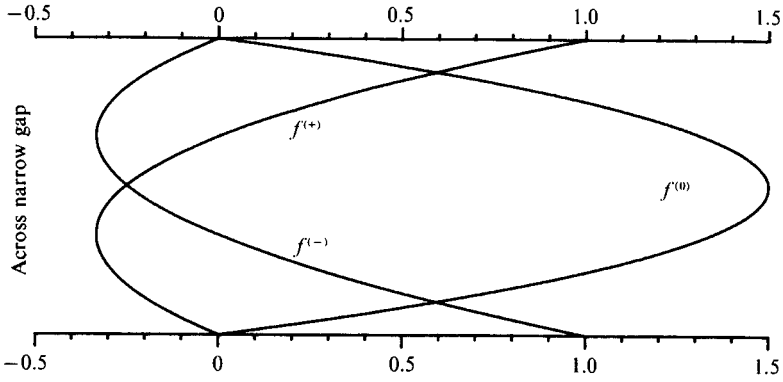

FIGURE 2. Profile functions $f^{(0)}, f^{(-)}, f^{(+)}$ associated respectively with the bulk flow, inner and outer boundary motion for a laminar flow in a narrow gap.

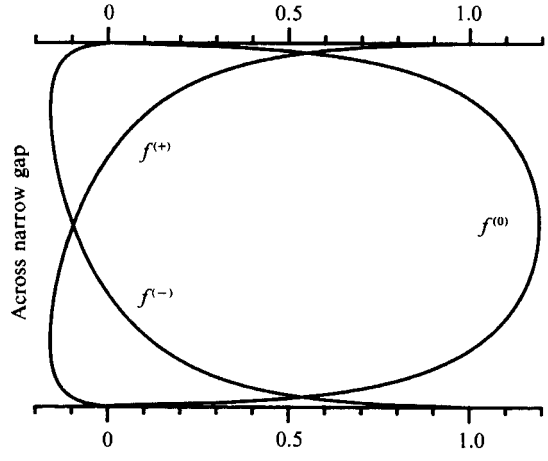

FIGURE 3. Profile functions $f^{(0)}, f^{(-)}, f^{(+)}$ associated respectively with the bulk flow, inner and outer boundary motion for a turbulent flow in a narrow gap with fractional roughness heights $\xi_*^{(-)} = \xi_*^{(+)} = 0.005$.

can be modelled by treating the turbulence as if it were merely a complicated sort of laminar flow with a parabolic viscosity

$$\mu = k\|\rho\|hu_*(\xi+\xi_*^{(-)})(1-\xi+\xi_*^{(+)}), \tag{6.8}$$

where k is von Kármán's constant, u_* is the friction velocity and the fractional roughness heights $\xi_*^{(-)}, \xi_*^{(+)}$ are exceedingly small (Elder 1959). The three velocity functions are all logarithmic (see figure 3):

$$f^{(0)} = 1+\frac{\delta^{(-)}(\ln(\xi+\xi_*^{(-)})+1)}{1-\delta^{(+)}-\delta^{(-)}}+\frac{\delta^{(+)}(\ln(1-\xi+\xi_*^{(+)})+1)}{1-\delta^{(+)}-\delta^{(-)}}, \tag{6.9a}$$

$$f^{(+)} = -\frac{\delta^{(+)}\delta^{(-)}(\ln(\xi+\xi_*^{(-)})+1)}{1-\delta^{(+)}-\delta^{(-)}}-\frac{\delta^{(+)}(1-\delta^{(-)})(\ln(1-\xi+\xi_*^{(+)})+1)}{1-\delta^{(+)}-\delta^{(-)}}, \tag{6.9b}$$

$$f^{(-)} = -\frac{\delta^{(-)}(1-\delta^{(+)})(\ln(\xi+\xi_*^{(-)})+1)}{1-\delta^{(+)}-\delta^{(-)}}-\frac{\delta^{(+)}\delta^{(-)}(\ln(1-\xi+\xi_*^{(+)})+1)}{1-\delta^{(+)}-\delta^{(-)}}, \tag{6.9c}$$

with

$$\delta^{(+)} = -1/\ln\xi_*^{(+)}, \quad \delta^{(-)} = -1/\ln\xi_*^{(+)}, \tag{6.9d, e}$$

where contributions of order $\xi_*^{(-)}, \xi_*^{(+)}$ have been neglected. Sometimes the logarithmic velocity profile is used to characterize this simple model for turbulence.

The stress vectors $\boldsymbol{\tau}^{(-)}, \boldsymbol{\tau}^{(+)}$ on the inner and outer surfaces are given by

$$[1-\delta^{(+)}-\delta^{(-)}]\boldsymbol{\tau}^{(-)} = \delta^{(-)} k u_* (\boldsymbol{U}_S - \boldsymbol{u}^{(-)} + \delta^{(+)}(\boldsymbol{u}^{(-)} - \boldsymbol{u}^{(+)})), \tag{6.10a}$$

$$[1-\delta^{(+)}-\delta^{(-)}]\boldsymbol{\tau}^{(+)} = \delta^{(+)} k u_* (\boldsymbol{U}_S - \boldsymbol{u}^{(+)} + \delta^{(-)}(\boldsymbol{u}^{(+)} - \boldsymbol{u}^{(-)})). \tag{6.10b}$$

By definition, the friction velocity u_* is related to the stress

$$u_*^4 = \tau^{(-)2} + \tau^{(+)2}. \tag{6.11}$$

So, even with this simplest of turbulence models the turbulence is coupled to the flow.

The representation (6.6) reduces the fluid dynamical problem from three to two spatial dimensions. For the laminar and for the turbulent flows, the departures from hydrostatic balance are given by the respective formulae

$$\nabla_S \|p\| - \|\rho\| \boldsymbol{g}_S = \frac{-12\mu}{h^2} (\boldsymbol{U}_S - \tfrac{1}{2}(\boldsymbol{u}^{(+)} + \boldsymbol{u}^{(-)})), \tag{6.12a}$$

$$\nabla_S \|p\| - \|\rho\| \boldsymbol{g}_S = \frac{-\|\rho\|}{h} (\boldsymbol{\tau}^{(-)} + \boldsymbol{\tau}^{(+)}). \tag{6.12b}$$

7. Shear dispersion tensor

For laminar flow with constant viscosity μ and diffusivity κ, it is now elementary to evaluate the shear dispersion tensor $\boldsymbol{D}_S$ as given by (5.1a, b):

$$\boldsymbol{D}_S = \frac{h^2}{210\kappa} \{ \boldsymbol{U}_S^{\mathrm{T}} \boldsymbol{U}_S - \tfrac{1}{2}(\boldsymbol{U}_S^{\mathrm{T}} \boldsymbol{u}_S^{(+)} + \boldsymbol{u}_S^{(+)\mathrm{T}} \boldsymbol{U}_S) - \tfrac{1}{2}(\boldsymbol{U}_S^{\mathrm{T}} \boldsymbol{u}_S^{(-)} + \boldsymbol{u}_S^{(-)\mathrm{T}} \boldsymbol{U}_S)$$
$$+ 2\boldsymbol{u}_S^{(+)\mathrm{T}} \boldsymbol{u}_S^{(+)} + 2\boldsymbol{u}_S^{(-)\mathrm{T}} \boldsymbol{u}_S^{(-)} - \tfrac{3}{2}(\boldsymbol{u}_S^{(+)\mathrm{T}} \boldsymbol{u}_S^{(-)} + \boldsymbol{u}_S^{(-)\mathrm{T}} \boldsymbol{u}_S^{(+)}) \}. \tag{7.1}$$

Thus, the bulk velocity and the motion of the boundaries all contribute to the shear dispersion. The positive-definite character of the tensor $\boldsymbol{D}_S$ is highlighted in the representation

$$\boldsymbol{D}_S = \frac{h^2}{210\kappa} (\boldsymbol{U}_S - \tfrac{1}{2}(\boldsymbol{u}_S^{(+)} + \boldsymbol{u}_S^{(-)}))^{\mathrm{T}} (\boldsymbol{U}_S - \tfrac{1}{2}(\boldsymbol{u}_S^{(+)} + \boldsymbol{u}_S^{(-)})) + \frac{h^2}{120\kappa} (\boldsymbol{u}_S^{(+)} - \boldsymbol{u}_S^{(-)})^{\mathrm{T}} (\boldsymbol{u}_S^{(+)} - \boldsymbol{u}_S^{(-)}). \tag{7.2}$$

The tensor products of the vectors give rise to the symmetric tensor form for $\boldsymbol{D}_S$. The two terms correspond to Poiseuille flow (Bugliarello & Jackson 1964, Appendix II, equation (4.5)) and to plane Couette flow (Saffman 1962, equation (17)).

For the turbulent (logarithmic velocity profile) case we invoke Reynolds' analogy and represent κ:

$$\kappa = \frac{\mu}{\|\rho\|} = k u_* h (\xi + \xi_*^{(-)})(1 - \xi + \xi_*^{(+)}). \tag{7.3}$$

If we neglect contributions of order $\xi_*^{(-)}, \xi_*^{(+)}$, then we need to evaluate the two weakly singular integrals (Elder 1959, (14); Gradshteyn & Ryzhik 1965, (4.221.1)):

$$\int_0^1 \frac{(1-\xi)(\ln(1-\xi))^2}{\xi} \mathrm{d}\xi = \int_0^1 \frac{\xi(\ln \xi)^2}{1-\xi} \mathrm{d}\xi = 0.40411, \tag{7.4a}$$

$$\int_0^1 \ln \xi \ln(1-\xi) \, \mathrm{d}\xi = 2 - \tfrac{1}{6}\pi^2 = 0.35506. \tag{7.4b}$$

The full expression for the shear dispersion tensor is

$$\boldsymbol{D}_S = 0.404\,11\,\frac{h}{k^3 u_*^3}\,(\boldsymbol{\tau}^{(-)\mathrm{T}}\boldsymbol{\tau}^{(-)} + \boldsymbol{\tau}^{(+)\mathrm{T}}\boldsymbol{\tau}^{(+)}) - (2-\tfrac{1}{6}\pi^2)\frac{h}{k^3 u_*^3}\,(\boldsymbol{\tau}^{(-)\mathrm{T}}\boldsymbol{\tau}^{(+)} + \boldsymbol{\tau}^{(+)\mathrm{T}}\boldsymbol{\tau}^{(-)}). \quad (7.5)$$

When one of the boundaries is unstressed, we recover the result derived by Elder (1959) for the longitudinal shear dispersion coefficient. The positive-definite character of $\boldsymbol{D}_S$ can be seen in the representation

$$\boldsymbol{D}_S = \tfrac{1}{2}(0.404\,11 - 2 + \tfrac{1}{6}\pi^2)\frac{h}{k^3 u_*^3}\,(\boldsymbol{\tau}^{(-)} + \boldsymbol{\tau}^{(+)})^{\mathrm{T}}(\boldsymbol{\tau}^{(-)} + \boldsymbol{\tau}^{(+)}) + \tfrac{1}{2}(0.404\,11 + 2 - \tfrac{1}{6}\pi^2)\,(\boldsymbol{\tau}^{(-)} - \boldsymbol{\tau}^{(+)})^{\mathrm{T}}(\boldsymbol{\tau}^{(-)} - \boldsymbol{\tau}^{(+)}). \quad (7.6)$$

The factor of 15.5 disparity in the coefficients shows that any mismatch in the stress vectors $\boldsymbol{\tau}^{(-)}, \boldsymbol{\tau}^{(+)}$ greatly enhances the shear dispersion.

The laminar and turbulent flows exhibit different scalings with gap width h and bulk velocity $\boldsymbol{U}_S$:

$$\boldsymbol{D} = O\left(\frac{(h|\boldsymbol{U}_S|)^2}{\kappa}\right) \quad \text{and} \quad \boldsymbol{D} = O(h|\boldsymbol{U}_S|). \quad (7.7a, b)$$

If the changes in gap width are in the main flow direction, then mass conservation (3.4) leads to $h|\boldsymbol{U}_S|$ remaining constant. So the scalings (7.7*a*, *b*) imply that the shear dispersion tensor will likewise remain constant even if there are substantial variations in gap width. Conversely, if the changes in gap width are orthogonal to the main flow direction (as in the example studied in §§9, 10), then $|\boldsymbol{U}_S|$ will be smallest where h is smallest. So, there will be exaggerated changes in shear dispersion coefficient in different parts of the flow field, particularly in the laminar case.

8. Principal values and directions

The formulae (7.2), (7.6) for the shear dispersion tensor $\boldsymbol{D}_S$ take the general form

$$\boldsymbol{D}_S = \alpha \boldsymbol{i}^{\mathrm{T}}\boldsymbol{i} + \beta \boldsymbol{j}^{\mathrm{T}}\boldsymbol{j}, \quad (8.1)$$

where α, β are positive scalars and $\boldsymbol{i}, \boldsymbol{j}$ are unit vectors. We denote the angle between these vectors as ψ (see figure 4). For laminar flows $\boldsymbol{i}$ is the direction of the plane Poiseuille flow and $\boldsymbol{j}$ is the direction of the Couette flow. For turbulent flows $\boldsymbol{i}$ is the direction of the sum of stresses and $\boldsymbol{j}$ the direction of the difference between the boundary stresses.

Unless $\boldsymbol{i}$ and $\boldsymbol{j}$ are orthogonal, the representation (8.1) is not in principal axes form. We seek the angle ϕ between a principal axis and the $\boldsymbol{i}$-direction. In component form, along and perpendicular to $\boldsymbol{i}$, the eigenvector equation is

$$\begin{pmatrix} \alpha + \beta\cos^2\psi & \beta\cos\psi\sin\psi \\ \beta\cos\psi\sin\psi & \beta\sin^2\psi \end{pmatrix}\begin{pmatrix}\cos\phi \\ \sin\phi\end{pmatrix} = \lambda\begin{pmatrix}\cos\phi \\ \sin\phi\end{pmatrix}, \quad (8.2)$$

where λ is the shear dispersion coefficient (eigenvalue) in the principal direction ϕ. The major (larger) and minor (smaller) values for λ are

$$\lambda = \tfrac{1}{2}(\alpha+\beta) \pm \tfrac{1}{2}[(\alpha+\beta)^2 - 4\alpha\beta\sin^2\psi]^{\frac{1}{2}}. \quad (8.3)$$

The major direction is given by

$$\tan\phi = \frac{\eta}{1+(1+\eta^2)^{\frac{1}{2}}}, \quad \text{with} \quad \eta = \frac{2\beta\sin\psi\cos\psi}{\alpha+\beta-2\beta\sin^2\psi}, \quad (8.4a, b)$$

with the minor direction at right angles to the major direction.

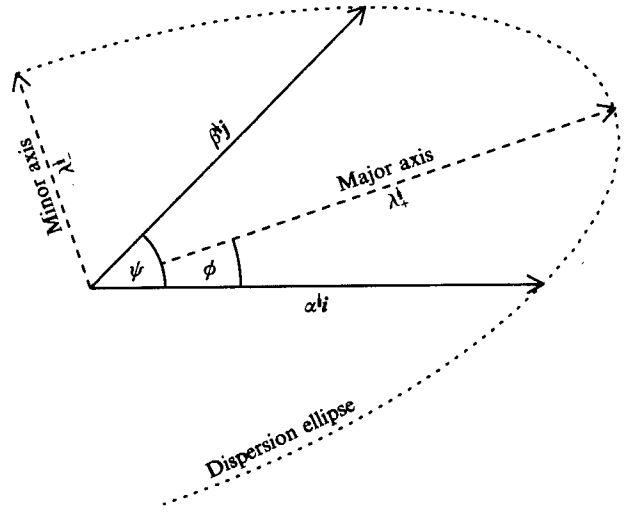

FIGURE 4. Definition sketch for the angle ψ between the directions i,j and for the angle ϕ of the major axis for shear dispersion.

In particular, when β is much smaller than α, we have

$$\lambda_+ = \alpha + \beta\cos^2\psi + \frac{\beta}{\alpha}\cos^2\psi\sin^2\psi + \ldots, \quad \lambda_- = \beta\sin^2\psi\left(1 - \frac{\beta}{\alpha}\cos^2\psi + \ldots\right), \tag{8.5a, b}$$

$$\tan\phi = \frac{\beta}{\alpha}\sin\psi\cos\psi\left(1 - \frac{\beta}{\alpha}(1 - 2\sin^2\psi) + \ldots\right). \tag{8.5c}$$

Hence the major shear dispersion coefficient is slightly increased from α, unless $\boldsymbol{j}$ is perpendicular to $\boldsymbol{i}$. The minor shear dispersion coefficient is critically dependent upon the angle ψ between the directions $\boldsymbol{i}$ and $\boldsymbol{j}$. The largest value occurs when $\boldsymbol{j}$ is perpendicular to $\boldsymbol{i}$. The major direction is slightly rotated from the $\boldsymbol{i}$-direction towards the $\boldsymbol{j}$-direction (unless these vectors $\boldsymbol{i},\boldsymbol{j}$ are parallel or perpendicular).

A physical interpretation of the dispersion ellipse, as shown in figure 4, is as the shape of a spot of dye a short time after discharge when shear dispersion $\boldsymbol{D}_S$ greatly dominates $\boldsymbol{K}_S$. The size of the dye cloud would scale as $(2t)^{\frac{1}{2}}$, until such times as it becomes large enough to experience any non-uniformities. The dye concentration varies inversely as the area of the dispersion ellipse.

In many circumstances it is desirable to achieve good mixing within the narrow gap, e.g. to avoid possible accumulation of debris. So, it would be advantageous to make the minor dispersion coefficient (8.5b) as large as possible. For a given (small) magnitude of β, this is achieved when the (secondary) direction $\boldsymbol{j}$ is perpendicular to the (primary) direction $\boldsymbol{i}$. When the plane Poiseuille flow dominates, the Couette flow should be directed orthogonally. When, the stresses $\boldsymbol{\tau}^{(-)}, \boldsymbol{\tau}^{(+)}$ are nearly equal, any difference in stress should be at right angles. So, in either the laminar or turbulent cases, it is best that any small boundary motions be orthogonal to the main flow direction.

9. Laminar flow around and along a journal bearing

To illustrate the application of the above general theory, we consider the steady situation where an imposed volume flow rate of lubricant is pumped along the non-uniform gap between a rotating cylindrical axle and a closely fitting stationary shaft. The same type of flow also arises in the boring of tunnels and in the drilling or lining of oil wells. We approximate the gap width by

$$h(\theta) = H(1-\epsilon\cos\theta), \tag{9.1}$$

where H is the nominal clearance and ϵH the displacement between two centres (see figure 5). The volume flow rate of lubricant is specified:

$$2\pi\overline{W}aH, \tag{9.2}$$

where a is the axle radius and $\overline{W}$ the nominal lubricant velocity along the axle.

The bulk velocity components around and along the axle are denoted $V_S(\theta), W_S(\theta)$. If we ignore density variations (and subtract the hydrostatic pressure), then the laminar momentum equation (6.12a) yields the two component equations

$$\frac{1}{\alpha}\partial_\theta\|p\| = -12\frac{\mu}{h^2}(V_S - \tfrac{1}{2}\Omega a), \tag{9.3a}$$

$$\partial_z\|p\| = -12\frac{\mu}{h^2}W_S, \tag{9.3b}$$

where Ω is the angular velocity of the axle rotation. For constant viscosity μ, it follows that the longitudinal velocity varies as the square of the gap width:

$$W_S = \overline{W}\frac{(1-\epsilon\cos\theta)^2}{1+\frac{3}{2}\epsilon^2}. \tag{9.4}$$

Figure 6 shows the relative change in $W_S(\theta)$ for $\epsilon = \frac{1}{4}, \frac{1}{2}, \frac{3}{4}$. Even for small fractional offset, the longitudinal flow tends to be confined to the region of greatest gap width.

The mass conservation equation (3.4) implies that the circulation

$$hV_S = \tfrac{1}{2}\Omega ah - \frac{h^3}{12\mu a}\partial_\theta\|p\| \tag{9.5}$$

is independent of θ. The periodicity of $\|p\|$ on going around the axle, enables us to evaluate the circulation and hence to solve for $V_S(\theta)$:

$$V_S = \frac{\Omega a(1-\epsilon^2)}{2(1-\epsilon\cos\theta)(1+\frac{1}{2}\epsilon^2)}. \tag{9.6}$$

When there is no offset ($\epsilon = 0$), the bulk velocity V_S around the axle is half the velocity $a\Omega$ of the axle. Figure 7 shows the relative change in $V_S(\theta)$ for increasing $\epsilon = \frac{1}{4}, \frac{1}{2}, \frac{3}{4}$. Although the mean velocity reduces with ϵ, the peak velocity exhibits a slight increase.

The formula (7.2) for the shear dispersion tensor $\boldsymbol{D}_S$ involves the Poiseuille and Couette flow vectors

$$\boldsymbol{U}_S - \tfrac{1}{2}(\boldsymbol{u}_S^{(+)} + \boldsymbol{u}_S^{(-)}) = \left(\frac{\Omega a\epsilon}{2(1-\epsilon\cos\theta)}\left[\cos\theta - \frac{3\epsilon}{2+\epsilon^2}\right], \frac{\overline{W}(1-\epsilon\cos\theta)^2}{1+\frac{3}{2}\epsilon^2}\right), \tag{9.7a}$$

$$\boldsymbol{u}_S^{(+)} - \boldsymbol{u}_S^{(-)} = \Omega a(-1, 0). \tag{9.7b}$$

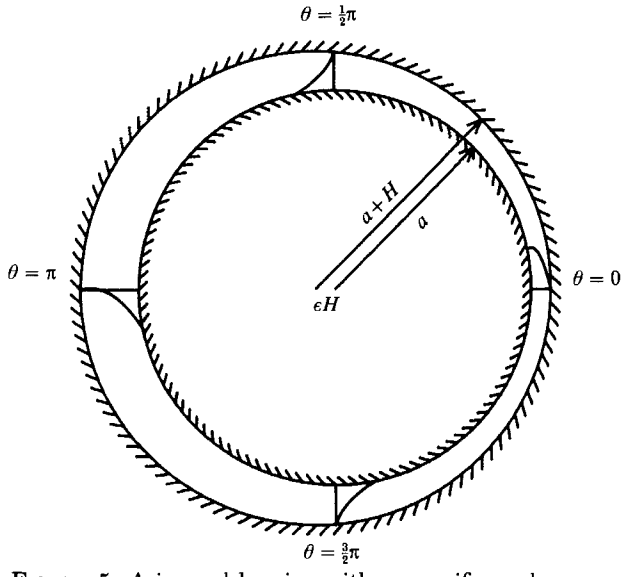

FIGURE 5. A journal bearing with non-uniform clearance.

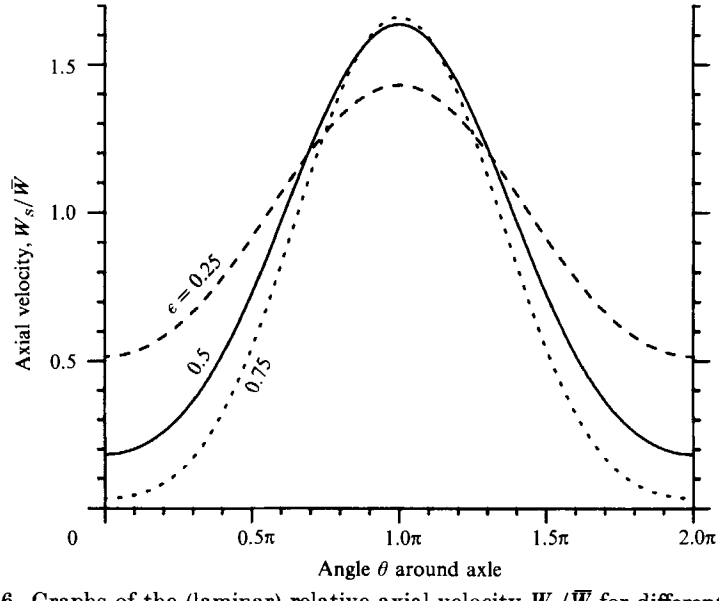

FIGURE 6. Graphs of the (laminar) relative axial velocity $W_s/\overline{W}$ for different values of the fractional offset ϵ between the centres of the axle and the shaft.

Thus in component form, we can evaluate the shear dispersion tensor:

$$D_{\theta\theta} = \frac{H^2\Omega^2a^2}{840\kappa}\left[\epsilon^2\left(\cos\theta - \frac{3\epsilon}{2+\epsilon^2}\right)^2 + 7(1-\epsilon\cos\theta)^2\right], \tag{9.8a}$$

$$D_{\theta z} = D_{z\theta} = \frac{H^2\overline{W}\Omega a}{420\kappa}\frac{\epsilon(1-\epsilon\cos\theta)^3}{(1+\frac{3}{2}\epsilon^2)}\left(\cos\theta - \frac{3\epsilon}{2+\epsilon^2}\right), \tag{9.8b}$$

$$D_{zz} = \frac{H^2\overline{W}^2}{210\kappa}\frac{(1-\epsilon\cos\theta)^6}{(1+\frac{3}{2}\epsilon^2)^2}. \tag{9.8c}$$

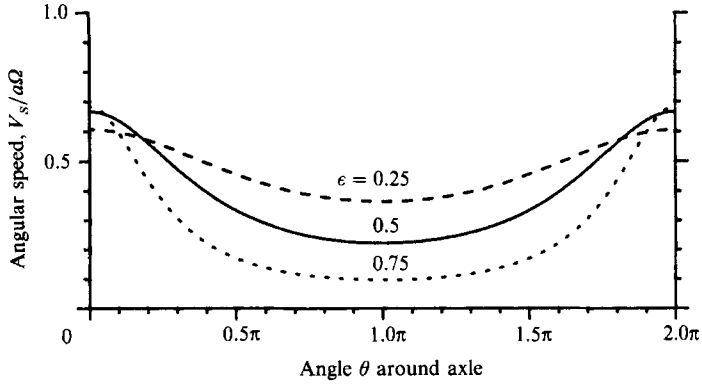

FIGURE 7. Graphs of the (laminar) relative angular speed $V_S/a\Omega$ for different values of the fractional offset ϵ between the centres of the rotating axle and the stationary shaft.

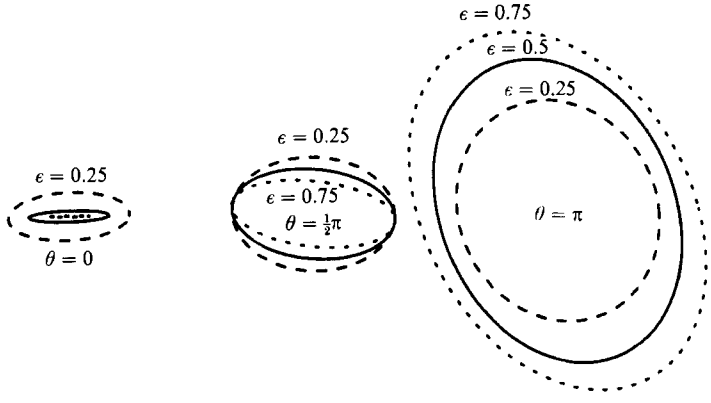

FIGURE 8. Dispersion ellipses showing how the (laminar) rate of shear dispersion is a function of direction, and varies with position θ around a journal bearing.

We note that in the concentric case $\epsilon = 0$ the principal directions are directed along and around the axle, even though the flow is helical. Figure 8 shows the relative sizes and orientations of the dispersion ellipses at the angular positions $\theta = 0, \frac{1}{2}\pi, \pi$ for $\epsilon = \frac{1}{4}, \frac{1}{2}, \frac{3}{4}$ with

$$\Omega a = \overline{W}. \tag{9.9}$$

The dominant feature is the exceedingly weak longitudinal dispersion at $\theta = 0$ where the gap is narrowest. Indeed, for $\epsilon = 0.75$ the longitudinal dispersion is imperceptible.

The components of $\boldsymbol{D}_S$ all have extrema at the widest (+) and narrowest (−) gap positions:

$$D_{\theta\theta} = \frac{H^2\Omega^2a^2}{840\kappa}\left[7 + \epsilon^2\left(\frac{1 \pm \frac{1}{2}\epsilon}{1 + \frac{1}{2}\epsilon^2}\right)^2\right](1 \pm \epsilon)^2, \tag{9.10a}$$

$$D_{\theta z} = D_{z\theta} = \frac{\mp H^2\overline{W}\Omega a\epsilon(1 \pm \frac{1}{2}\epsilon)}{420\kappa(1 + \frac{3}{2}\epsilon^2)(1 + \frac{1}{2}\epsilon^2)}(1 \pm \epsilon)^4, \tag{9.10b}$$

$$D_{zz} = \frac{H^2\overline{W}^2(1 \pm \epsilon)^6}{210\kappa(1 + \frac{3}{2}\epsilon^2)}. \tag{9.10c}$$

For $\epsilon = 0.75$ the longitudinal dispersion D_{zz} varies by the extremely large factor 7^6 between the narrowest and widest gaps, while the transverse dispersion $D_{\theta\theta}$ varies by

the more modest factor 55. As the gap closes (i.e. as $1-\epsilon$ tends to zero), all the shear dispersion components tend to zero. However, the rates of decay $(1-\epsilon)^2, (1-\epsilon)^4$, $(1-\epsilon)^6$ are quite distinct. For narrow gaps $D_{\theta\theta}$ dominates if Ωa exceeds $\frac{1}{2}(1-\epsilon)^2 W$. So, rotation of the axle becomes particularly important if one seeks to avoid possible accumulation of debris where the gap is small.

There is quadratic dependence of $D_{\theta\theta}$ upon the angular velocity Ω. So doubling Ω would double the lateral width of the dispersion ellipses as shown in figure 8, and would halve the time for there to be significant mixing around the axle and for the dispersion process to evolve towards its next stage of one-dimensional longitudinal dispersion (Taylor 1953).

10. Turbulent flow around and along a journal bearing

In the turbulent (logarithmic velocity profile) case we have the major additional difficulty that the turbulence level, as typified by $u_*(\theta)$, is itself a function of the unknown velocity field. The stresses (6.10a, b) at the two surfaces are given by

$$(1-\delta^{(+)}-\delta^{(-)})\,\tau^{(-)} = \delta^{(-)} k u_* (V_S - a\Omega(1-\delta^{(+)}), W_S), \tag{10.1a}$$

$$(1-\delta^{(+)}-\delta^{(-)})\,\tau^{(+)} = \delta^{(+)} k u_* (V_S - \delta^{(-)} a\Omega, W_S), \tag{10.1b}$$

where

$$\delta^{(+)} = -1/\ln \xi_*^{(+)}, \quad \delta^{(+)} = -1/\ln \xi_*^{(-)}. \tag{10.1c, d}$$

So, the definition (6.11) for u_* becomes

$$(1-\delta^{(+)}-\delta^{(-)})^2 u_*^4 = k^2 u_*^2 \{\delta^{(-)2}(V_S - a\Omega(1-\delta^{(+)}))^2 + \delta^{(+)2}(V_S - \delta^{(-)} a\Omega)^2\} + (k u_* W_S)^2 \{\delta^{(+)2} + \delta^{(-)2}\}. \tag{10.2}$$

Before we can solve this equation for $u_*(\theta)$ we need to determine V_S and $u_* W_S$. To avoid undue complication, we shall regard the fractional roughness heights $\xi_*^{(-)}, \xi_*^{(+)}$ as being constants.

For constant-density flows (with the hydrostatic pressure subtracted), the momentum equation (6.12b) yields the two component equations

$$(1-\delta^{(+)}-\delta^{(-)}) \frac{H}{a\|\rho\|} \partial_\theta \|p\| = \frac{-ku^*}{1-\epsilon\cos\theta} ((\delta^{(+)}+\delta^{(-)})\, V_S - \delta^{(-)} a\Omega), \tag{10.3a}$$

$$(1-\delta^{(+)}-\delta^{(-)}) \frac{H}{\|\rho\|} \partial_z \|p\| = \frac{-k u_* W_S}{1-\epsilon\cos\theta} (\delta^{(+)}+\delta^{(-)}). \tag{10.3b}$$

If the velocities are independent of z, then we can infer that $u_* W_S$ can be represented as

$$u_* W_S = \overline{W}(1-\epsilon\cos\theta)\, 2\pi \Big/ \int_0^{2\pi} u_*^{-1} (1-\epsilon\cos\theta)^2 \,\mathrm{d}\theta, \tag{10.4}$$

where $\overline{W}$ is the mean velocity along the axle.

As in the laminar case there is a constant circulation

$$(1-\epsilon\cos\theta)\, V_S = a\Omega \frac{(1-\epsilon\cos\theta)\,\delta^{(-)}}{\delta^{(+)}+\delta^{(-)}} + (1-\epsilon\cos\theta)^2 \frac{H}{a\|\rho\|} \partial_\theta \|p\| \frac{(1-\delta^{(+)}-\delta^{(-)})}{\delta^{(+)}+\delta^{(-)}}. \tag{10.5}$$

The periodicity of $\|p\|$ with respect to θ enables us to obtain the solution

$$(1-\epsilon\cos\theta)\,V_S(\theta) = \frac{a\Omega\delta^{(-)}}{\delta^{(+)}+\delta^{(-)}}\int_0^{2\pi} u_*(1-\epsilon\cos\theta)^{-1}\,\mathrm{d}\theta \Big/ \int_0^{2\pi} u_*(1-\epsilon\cos\theta)^{-2}\,\mathrm{d}\theta. \tag{10.6}$$

In particular, when there is no offset ($\epsilon = 0$) and the inner and outer fractional roughness heights are equal ($\delta^{(-)} = \delta^{(+)}$), the bulk velocity V_S around the axle is half the velocity $a\Omega$ of the axle.

The solutions (10.4), (10.6) for $u_*\,W_S$ and V_S in terms of $u_*(\theta)$ allow us to regard (10.2) as being a quartic for $u_*(\theta)$:

$$u_*^4 = u_*^2\,a^2\Omega^2 A(\theta) + \overline{W}^2 B(\theta)^2. \tag{10.7}$$

The coefficients $A(\theta), B(\theta)$ are functionals of $u_*(\theta)$:

$$\begin{aligned}
&[1-\delta^{(+)}-\delta^{(-)}]^2\,(1-\epsilon\cos\theta)^2\frac{A}{k^2} \\
&= \delta^{(-)2}\left\{(1-\epsilon\cos\theta)\,(1-\delta^{(-)}) - \frac{\delta^{(-)}}{\delta^{(+)}+\delta^{(-)}}\int_0^{2\pi} u_*(1-\epsilon\cos\theta)^{-1}\,\mathrm{d}\theta \Big/ \int_0^{2\pi} u_*(1-\epsilon\cos\theta)^{-2}\,\mathrm{d}\theta\right\}^2 \\
&\quad + \delta^{(+)2}\left\{-(1-\epsilon\cos\theta)\,\delta^{(+)} + \frac{\delta^{(-)}}{\delta^{(+)}+\delta^{(-)}}\int_0^{2\pi} u_*(1-\epsilon\cos\theta)^{-1}\,\mathrm{d}\theta \Big/ \int_0^{2\pi} u_*(1-\epsilon\cos\theta)^{-2}\,\mathrm{d}\theta\right\}^2,
\end{aligned} \tag{10.8a}$$

$$(1-\delta^{(+)}-\delta^{(-)})\frac{B}{k} = (1-\epsilon\cos\theta)\,\{\delta^{(-)2}+\delta^{(+)2}\}^{\frac{1}{2}}\,2\pi \Big/ \int_0^{2\pi} u_*^{-1}(1-\epsilon\cos\theta)^2\,\mathrm{d}\theta. \tag{10.8b}$$

The unique positive solution for $u_*(\theta)$ is

$$u_* = \{\tfrac{1}{2}a^2\Omega^2 A + [\overline{W}^2 B^2 + \tfrac{1}{4}a^4\Omega^4 A^2]^{\frac{1}{2}}\}^{\frac{1}{2}}. \tag{10.9}$$

For the concentric case $\epsilon = 0$ the friction velocity u_* is independent of the angular θ:

$$\begin{aligned}
&(1-\delta^{(+)}-\delta^{(-)})^2\frac{u_*^2}{k^2} \\
&= a^2\Omega^2\left\{\left(\frac{\delta^{(+)}\,\delta^{(-)}}{\delta^{(+)}+\delta^{(-)}} - \delta^{(-)2}\right)^2 + \left(\frac{\delta^{(+)}\,\delta^{(-)}}{\delta^{(+)}+\delta^{(-)}} - \delta^{(+)2}\right)^2\right\} + \overline{W}^2\{\delta^{(-)2}+\delta^{(+)2}\}.
\end{aligned} \tag{10.10}$$

So, the turbulence is dependent both upon the angular velocity $a\Omega$ of the axle and upon the bulk flow velocity $\overline{W}$ along the axle.

A robust iterative computational scheme to solve for $u_*(\theta)$ is to begin with a starting function $u_*^{(0)}(\theta)$, such as the concentric solution (10.10). At the mth stage the approximation $u_*^{(m)}(\theta)$ is used in (10.8*a*, *b*) to evaluate the functionals $A^{(m)}(\theta)$, $B^{(m)}(\theta)$. The corresponding solution of (10.9) is denoted $u_*^{(m+1)}(\theta)$. The iterations continue until the fractional difference between successive iterates $u_*^{(m)}, u_*^{(m+1)}$ is acceptably small. Figure 9 shows the relative change in $u_*(\theta)$ for several values of ϵ in the case

$$a\Omega = \overline{W}, \quad \xi_*^{(-)} = \xi_*^{(+)} = 0.005, \quad \delta^{(-)} = \delta^{(+)} = 0.189. \tag{10.11a, b, c}$$

The uniformity of u_* around the axle can be attributed to the compensating effects of decreasing circulation velocity V_S where the longitudinal velocity W_S increases.

Once $u_*(\theta)$ is known, we can use (10.4), (10.6) to evaluate the axial and circumferential velocities W_S and V_S (see figures 10, 11). It is noteworthy that for the axial velocity W_S, the changes with ϵ are less marked than in the laminar case.

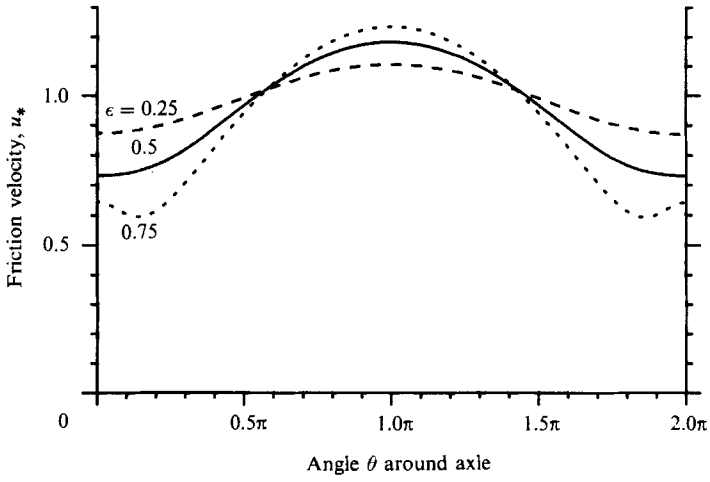

FIGURE 9. Graph of the friction velocity u_* (relative to that in the concentric case $\epsilon = 0$) as a function of position θ around a journal bearing.

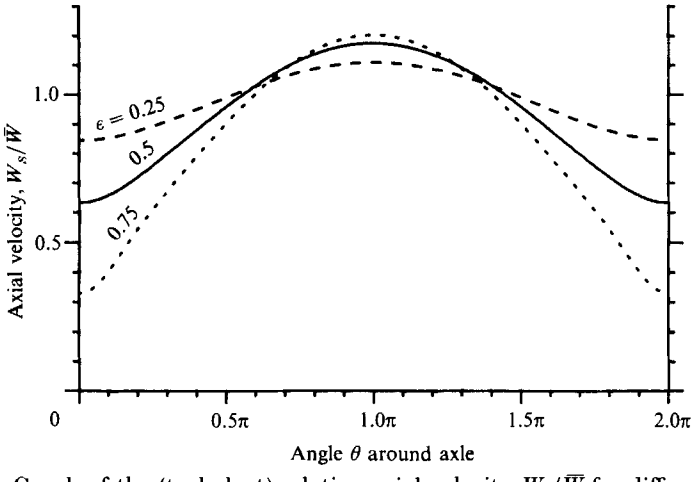

FIGURE 10. Graph of the (turbulent) relative axial velocity $W_s/\overline{W}$ for different values of the fractional offset ϵ between the centres of the axle and the shaft.

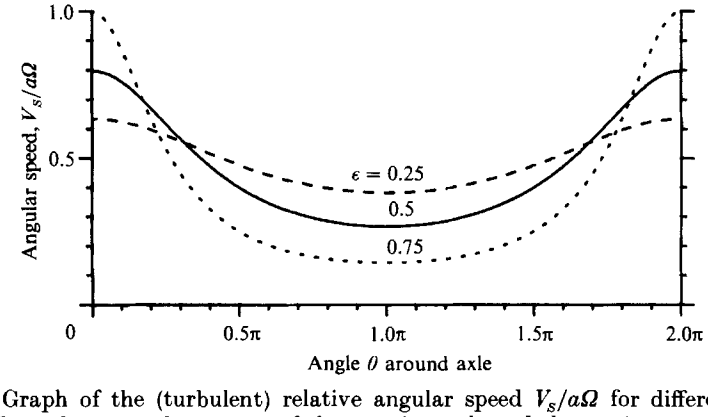

FIGURE 11. Graph of the (turbulent) relative angular speed $V_s/a\Omega$ for different values of the fractional offset ϵ between the centres of the rotating axle and the stationary shaft.

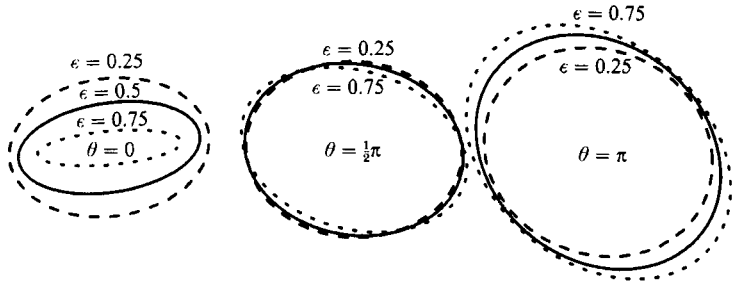

FIGURE 12. Dispersion ellipses showing how the (turbulent) rate of shear dispersion is a function of direction, and varies with position θ around a journal bearing.

Next, from (10.1*a*, *b*) we can evaluate the stresses $\boldsymbol{\tau}^{(-)}, \boldsymbol{\tau}^{(+)}$ on the inner and outer surfaces. The formulae (7.5) or (7.6) permit us to evaluate the shear dispersion tensor $\boldsymbol{D}_S$. For the concentric case $\epsilon = 0$, and with equal values of the roughness heights

$$\xi_*^{(-)} = \xi_*^{(+)} = \xi_*, \quad \delta_* = -1/\ln \xi_* \tag{10.12a, b}$$

we have the explicit formulae

$$D_{\theta\theta} = \frac{H\delta_*}{k^2}(0.404\,11 + 2 - \tfrac{1}{6}\pi^2)\frac{\frac{1}{2}a^2\Omega^2}{\{\frac{1}{2}a^2\Omega^2 + 2\hat{W}^2\}^{\frac{1}{2}}}, \tag{10.13a}$$

$$D_{\theta z} = D_{z\theta} = 0, \tag{10.13b}$$

$$D_{zz} = \frac{H\delta_*}{k^2}(0.404\,11 - 2 + \tfrac{1}{6}\pi^2)\frac{2\hat{W}^2}{\{\frac{1}{2}a^2\Omega^2 + 2\hat{W}^2\}^{\frac{1}{2}}}, \tag{10.13c}$$

with

$$\hat{W} = \overline{W}/(1 - 2\delta_*). \tag{10.13d}$$

So, as in the laminar case, the principal directions are along and around the axle even though the flow is helical. The factor of 15.5 disparity in the numerical coefficients makes the two-dimensional dispersion process sensitive to the rotation velocity $a\Omega$ of the axle. For example,

$$D_{\theta\theta} = D_{zz} \quad \text{when} \quad a\Omega = 0.508\overline{W}, \tag{10.14}$$

even though the velocity around the axle is only a quarter of the longitudinal velocity.

The corresponding isotropic model for the turbulent diffusivity $\boldsymbol{K}$ is

$$K_{\theta\theta} = K_{zz} = 0.15kH\delta_*\{\tfrac{1}{2}a^2\Omega^2 + 2\hat{W}^2\}^{\frac{1}{2}}. \tag{10.15}$$

Fischer (1978, 5.1.1.2) discusses the evidence for the empirical factor 0.15. If we take the von Kármán constant to have the value $k = 0.4$, then

$$D_{\theta\theta} \geqslant K_{\theta\theta} \quad \text{if} \quad a\Omega \geqslant 0.2226\overline{W}, \tag{10.16}$$

$$D_{zz} \geqslant K_{zz} \quad \text{if} \quad 4.05\overline{W} \geqslant a\Omega. \tag{10.17}$$

So, when the velocity around the axle exceeds about one-ninth of the longitudinal velocity, the shear dispersion $D_{\theta\theta}$ in the axial direction exceeds the turbulent diffusivity $K_{\theta\theta}$. However, when the flow is principally around the axle, it requires a longitudinal velocity greater than half the velocity around the axle for shear dispersion D_{zz} to exceed K_{zz}. It is the quadratic dependence of the shear dispersion

coefficients $D_{zz}, D_{\theta\theta}$ upon $\overline{W}$ and $a\Omega$ that makes the two-dimensional dispersion process change in character over such a modest range of the ratio $a\Omega/\overline{W}$.

Figure 12 shows the relative sizes and orientations of the dispersion ellipses for three values of ϵ and three angular positions θ in the case (10.11 *a*, *b*, *c*). The changes with ϵ are less marked than in the laminar case. There is, however, a clear transition between transverse shear dispersion at the narrowest part ($\theta = 0$) and isotropic shear dispersion at the widest part ($\theta = \pi$). So, as in the laminar case, rotation of the axle is particularly important when the gap is narrow if accumulation of debris is to be avoided.

I wish to express my thanks to Simon Bittleston, Peter Long and Ian Walton of Schlumberger Cambridge Research, to whom miscible Newtonian fluids are but an elementary special case. This work was financed by The Royal Society.

REFERENCES

Aris, R. 1956 On the dispersion of a solute in a fluid through a tube. *Proc. R. Soc. Lond.* A **235**, 67–77.

Bugliarello, G. & Jackson, E. D. 1964 Random walk study of convective diffusion. *Engng Mech. Div. ASCE* **90**, 49–77.

Csanady, G. T. 1969 Diffusion in an Ekman layer. *J. Atmos. Sci.* **26**, 414–475.

Elder, J. W. 1959 The dispersion of marked fluid in turbulent shear flow. *J. Fluid Mech.* **5**, 544–560.

Fischer, H. B. 1978 On the tensor form of the bulk dispersion coefficient in a bounded skewed shear flow. *J. Geophys. Res.* **83**, 2373–2375.

Gradshteyn, I. S. & Ryzhik, I. M. 1965 *Tables of Integrals, Series and Products.* Academic Press.

Hamrick, J. M. 1986 Long-term dispersion in unsteady skewed free surface flow. *Estuarine, Coastal Shelf Sci.* **23**, 807–845.

Saffman, P. G. 1962 The effect of wind shear on horizontal spread from an instantaneous ground source. *Q. J. R. Met. Soc.* **88**, 382–393.

Smith, F. B. 1965 The role of wind shear in horizontal diffusion of ambient particles. *Q. J. R. Met. Soc.* **91**, 318–329.

Smith, R. 1979 Buoyancy effects upon lateral dispersion in open-channel flow. *J. Fluid Mech.* **90**, 761–779.

Taylor, A. D. 1982 Puff growth in an Ekman layer. *J. Atmos. Sci.* **39**, 837–850.

Taylor, G. I. 1953 Dispersion of soluble matter in solvent flowing slowly through a tube. *Proc. R. Soc. Lond.* A **219**, 186–203.